Modeling and analysis of a low loss Hexa circular PC-PCF for efficient THz waveguide transmission

MD. AMINUL ISLAM, MOHAMMAD RAKIBUL ISLAM[*], ZAREEN MUSTAFA, AADREETA HOSSAIN, TAHIA TAHSIN
Department of Electrical and Electronic Engineering, Islamic University of Technology, Gazipur1704, Bangladesh

In this paper, a porous-core photonic crystal fiber (PC-PCF) is proposed to minimize the effective material loss for terahertz wave transmission. The full vector finite element method with an ideally matched layer boundary condition is used to characterize the wave guiding properties of the proposed fiber. At an operating frequency of 0.5-1.7 THz, simulated results exhibit an extremely low effective material loss of 0.029 cm⁻¹, high core power fraction of 50% and ultra-flattened dispersion of 1.03 ± 0.04 ps/THz/cm at 90% porosity. Besides, only circular air holes have been used which makes the fiber remarkably simpler. Also, physical insights of the proposed fiber have been discussed. The proposed fiber has the potential of being a promising candidate for different applications in the THz regime.

1. Introduction

During the last decade, terahertz radiation spectrum has been the center of attention for many scientists and researchers due to its wide use in multidisciplinary fields including medical imaging, biomedical sensing, terahertz time-domain spectroscopy, and security applications. Massive evolution has already been attained in prototyping coherent terahertz sources and detectors. Nonetheless, drafting of compressed and low-loss terahertz waveguides are existent provocations for the terahertz research community all over the world. The diverse range of structures including metallic waveguides, dispersionless parallel-plate waveguides, metalized glass tubes, plastic ribbon waveguides, and metallic wire has already been suggested for effective transmission of terahertz waves.

Photonic Crystal Fiber (PCF) has been the core of attention for engineers and researchers in recent years due to its diversity in designing with comparison to the conventional optical fibers. PCF has become such an integrated field of research since its uses and development are included in biomedical and industrial sectors along with telecommunication and non-telecommunication sectors. Uses of PCF in modern times include THz telecommunications, nonlinear optics, biosensing, chemical sensing, spectroscopy, optical chromatography, fuel adulteration detection, bio-photonics and neurophotonics, cancer cell detection, HIV viral load detection, protein detection, diabetics detection etc. The core structure of PCFs is some periodically or arbitrarily placed air-holes which, together, cover the whole length of the fiber. The structure of PCF is so robust that it can be formed into multiple geometric structures including D-shape, pentagonal, tapered, panda-shaped, colloidal, spherical, rhombic, decagonal, circular honeycomb cladding and spiral.

However, the first-ever structure of PCF concocted was the Hexagonal PCF by Knight et al in 1996[1]. The prime area of research is the guiding properties of PCF which eventually resulted in a thriving performance. Wavelength [2], Phase [3] and Polarization of light [4] are some of the parameters which affect the guiding properties of PCF.

After the presentation of the idea of a PCF by Yeh et al in 1978 [5], it has come a long way by gaining characteristics like high relative sensitivity [6], low confinement loss [7], high numerical aperture [8], high nonlinearity [9], high birefringence [9], large mode area [10], low bending loss [11], ultralow material loss of THz waveguide [12], ultra-flat dispersion [13] and zero-flat dispersion [14] by altering the air hole diameters and pitch by modification throughout the years. The light-guiding process categorizes the PCF into two classes as Photonic Gap Fiber [15] which uses photonic band gap effect to guide the light throughout the length of the fiber and Total Internal Reflection (TIR) is used in this class which is a common optical property and it is called TIR-PCF [16]. Furthermore, it allows many facilities during fabrication [17]. It is an ordinary operation to impound fundamental mode power into the porous air holes, as dry air is predominantly insensitive to terahertz waves.

Some of the background materials which have been used to develop the guiding properties of PCF are Silica [18], PMMA [19], Teflon [20], Topaz [21] and Tellurite [22]. Amid these, Topaz is the most fitting choice, since it has low bulk material absorption loss [23] and manifests an almost constant refractive index over 0.1–2 THz frequency bands [24]. Also, it is humidity-insensitive [25], good for biosensing [26], photosensitive [27], and can be drawn together with Zeonex to make step-index fibers [27].

Many recognizable PC-PCFs have already been designed over two decades by the researchers to obtain guiding properties such as low confinement loss, low EML, and high-power fraction into porous air holes. In 2018, a circular structured photonic crystal fiber, at the porosity of 80% and a diameter of 304 μm had been reported with a very low effective material loss of 0.046 cm^{-1} at 1.01 THz. However, the highest power fraction noted, in this case, was 26.82% and 28.32% attained at 320 um for both x-pole and y-pole respectively which are both low in comparison to other designs [28]. Another circle-based star shape photonic crystal fiber (CS-PCF) has been proposed for terahertz (THz) spectrum that exhibits an extremely-low material loss of 0.01607 cm^{-1} and a large effective area of 1.386×10^6 μm^2 at 1.0 THz frequency with 55% core porosity, which might face complications during fabrication because of its complex structure [29].

Later in 2019, several designs having unprecedented waveguide properties have been developed lately. In particular, a square lattice porous core microstructure fiber is proposed displaying low effective absorption loss of 0.06 cm^{-1}, low bending loss of 8.8×10^{-9} dB/m, and core power fraction of 47% through the core at 1THz simultaneously, though this structure shows some prominent results, it concludes high confinement loss of 9.2×10^{-3} cm^{-1}. Moreover, low dispersion variation of 0.85 ± 0.12 ps/THz/cm over a range of frequency from 0.7 to 1.15 THz is found in this structure [30]. Later on, a conventional hexagonal cladding PCF demonstrated near zero dispersion coefficient of 0.47 ps/THz/cm at 300μm core diameter, with high porosity of 85%, an operating frequency of 1.3 THz, an effective material loss value of 0.039 cm^{-1} and high confinement loss of 7.8×10^{-4} cm^{-1} which shows similar problems like the square-lattice porous core microstructure fiber [31]. Another design

featuring decagonal cladding and hexagonal porous core was proposed that offers effective material loss of 0.0492cm^{-1} along with a high core power fraction of 43% for an operating frequency of 1THz, 81.5% core porosity, in addition it has confinement loss in the range of 10^{-4} to 10^{-2} which is high and the operating frequency range is very small standing at .9 to 1.25 THz [32].

Continuing the research in 2020, a diverse range of structures have flourished with unrivalled waveguide properties. Isolating a single structure, an octagonal shaped cladding with octagonal-shaped air holes and rectangular slotted core with outstanding results including effective material loss at 0.007 cm^{-1}, confinement loss at 10^{-15} cm^{-1}, core power fraction at 70% and dispersion at 0.3±0.1 ps/THz/cm was proposed. Though this structure has prominent results, in reality it will be difficult to fabricate such a complex and delicate structure [33].

In this paper, we have proposed a new design that consists of a hexagon-shaped porous-core with regular lattice and circular air holes in the cladding. Here, Topaz is used as background material and the fiber structure is kept very simple for fabrication purposes. Among the different cladding structures already proposed, the circular air hole cladding gives low dispersion than polygonal cladding with a similar result in air filling fractions [34]. The proposed design exhibits extremely low confinement loss, low effective material loss, high core power fraction along with a wide range of low flattened dispersion.

2. Structure of the proposed PCF

A noble structure of photonic crystal fiber has been suggested to minimize the effective material loss. The cross-sectional panorama of the proposed design is displayed in Fig. 1.
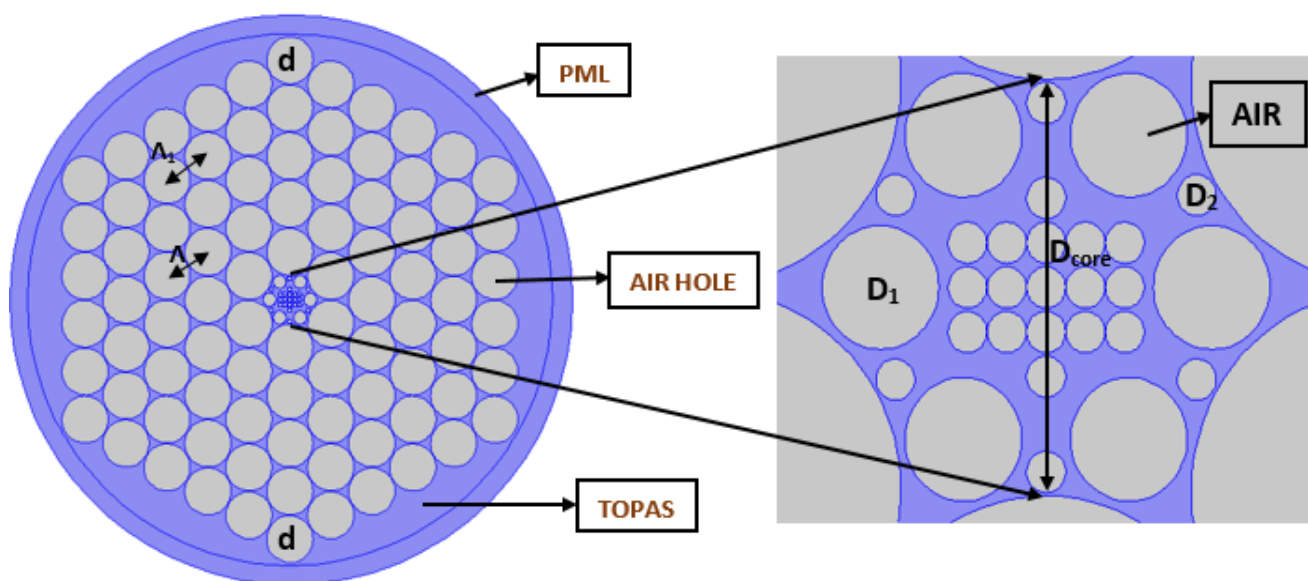

Fig. 1. Cross-section of the proposed porous-core THz fiber with TOPAS as the background material. An enlarged view of the porous core is shown in the inset (color online)

Five rings are used for hexagon cladding structure. The diameter of each air hole in the cladding is denoted by d. In the cladding the center to center distance between two adjacent circular air holes is denoted by Λ and Λ_1. The distance between two adjacent air holes lies in the same ring are denoted by Λ_1 and that lies in the other ring denoted by Λ. They are connected with each other by $\Lambda_1 = 0.98 \Lambda$. The diameter of the proposed core structure is demonstrated by D. The core structure of the proposed design is a combination of six large air holes which is denoted by D_1 and 23 small air holes which are denoted by D_2 respectively. The diameter of the D_1 is forty-two times of porosity and the diameter of the D_2 is fourteen times of porosity. Topaz has been used as a background material of this proposed fiber because it offers superior glass transition temperature than Zeonex and also it has lower bulk material absorption loss than PMMA and Teflon. The structure of our proposed photonic crystal fiber (PCF) is designed and theoretically investigated using full vector finite element method (FEM) based software COMSOL Multiphysics v5.3a. To absorb the scattered electromagnetic waves toward the surface, a perfectly matched layer (PML) is used outside the cladding area and the thickness of the PML region used for the calculation is about 7% of the total fiber radius. User-controlled mesh size was used for getting the best result in this fiber. The complete mesh of the fiber consists of 81606 elements, 7684 boundary elements, 484 vertex elements and the number of degrees of freedom solved for 571691 and the average element quality was 0.8254 and the minimum element quality was 0.4031. The element area ratio is 2.095E-5 and mesh area is 8380000 μm^2. Also some parameters are input display precision is 5 and output precision is 6. For sketching grid, the column width = 100 and the row height = 20.

(a)   *(b)*   *(c)*   *(d)*   *(e)*   *(f)*
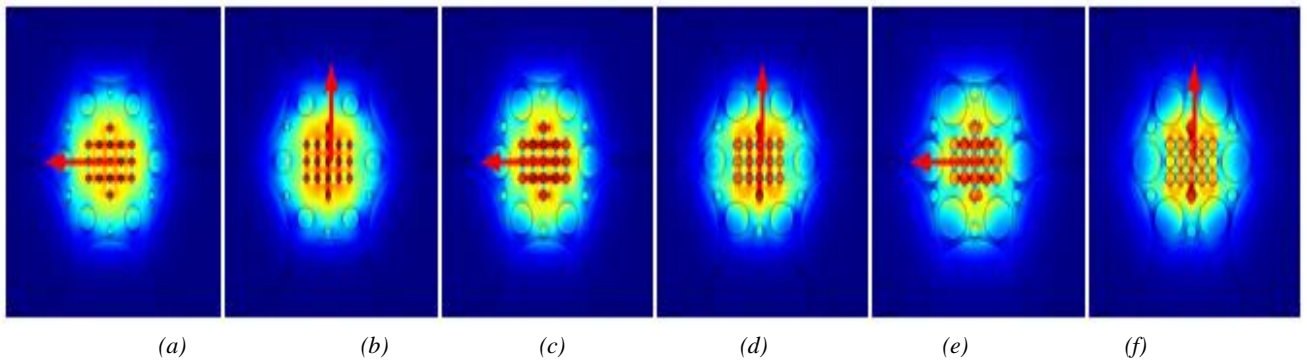
Fig. 2. Mode field profiles of the proposed fiber for x-polarization (Fig.a) and y-polarization (Fig.b) at 50% porosity respectively, x-polarization (Fig.c) and y-polarization (Fig.d) at 70% porosity, x-polarization(Fig.e) and y-polarization(Fig.f) at 90% porosity (color online)

Fig. 2 shows the mode field distributions of the proposed PCF for both x-polarization and y-polarization at different core porosities. It is clearly evident from the figure that the mode power is tightly confined within the porous core, which is essential for the transmission of THz waves. As the porosity is increased, the difference in refractive index between the core and the cladding reduces. As a result, the mode field starts to spread out towards the cladding region, which can be observed from the figure.

3. Simulation results

The vast majority of the polymer materials are exceedingly absorbent in the THz frequency region and efficient transmission of THz sign is generally constrained effective material loss (EML). In order to have proficient transmission EML must be of low value. Analysis of the absorption loss is first investigated with the help of the following analytical expression [47]

$$\alpha_{eff} = \sqrt{\frac{\varepsilon_0}{\mu_0}} \left(\frac{\int_{mat} n_{mat} |E|^2 \alpha_{mat} dA}{\left| \int_{all} S_z dA \right|} \right) \quad (1)$$

where α_{mat} symbolizes bulk material absorption loss, n_{mat} symbolizes the effective refractive index, ε_o and μ_o is the relative permittivity and permeability of vacuum respectively. The amount and direction of electromagnetic power enumerated by the following expression [48]

$$S_z = \frac{1}{2} \times (E \times H^*) \quad (2)$$

where E is the electric field component and H^* is complex conjugate of the magnetic field component. S_z is the pointing vector of z-component.
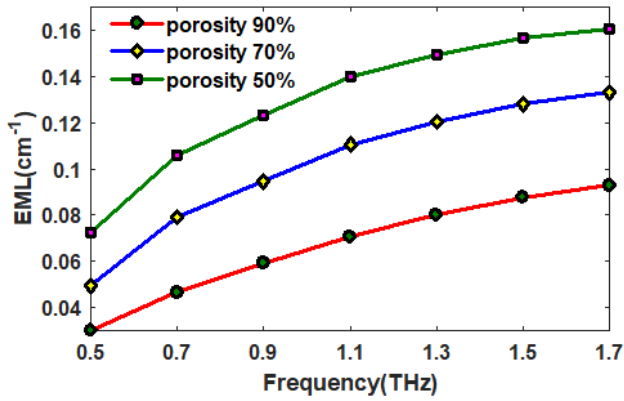
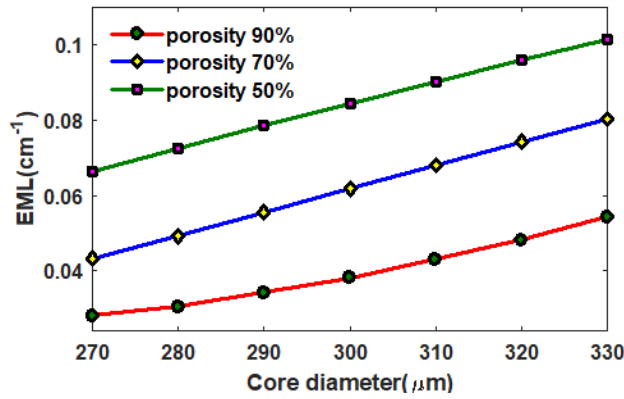*Fig. 3. Effective material loss vs frequency at different core porosities (color online)*

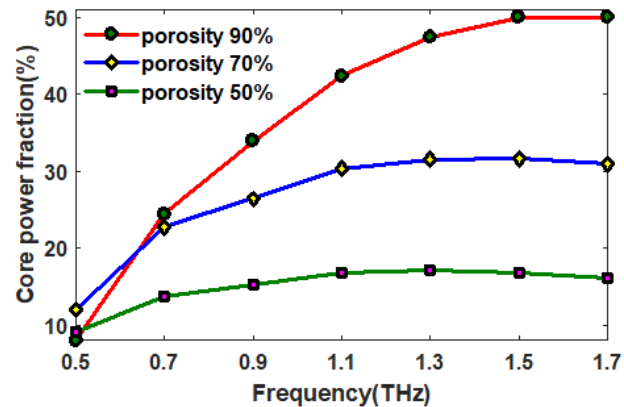*Fig. 4. Effective material loss vs core diameter at different core porosities (color online)*

Fig. 5. Core power fraction vs frequency at different core porosities (color online)

Effective material loss is proportional to electromagnetic wave frequency thus it changes significantly with addition in frequency. From Fig. 3 we can see that increase in frequency increases EML. On the contrary, Fig. 4 represents decreasing EML when core porosity and core diameter are increased. The reason is, at higher core porosity, a portion of background material is diminished and the mode power streams to a greater extent through the circular air slots creating reduction in EML.

Likewise, when the core diameter is expanded light gets less in contact with the material hence bulk absorption loss decreases. Simulation result shows that at 290μm core diameter, with a high porosity of 90%, the proposed fiber demonstrates an ultra-low effective material loss value of 0.029 cm^{-1}.

Apart from lower effective material loss, high core power fraction is expected while designing a standard THz waveguide. Core power fraction states the amount of power promulgating through the porous core. It can be estimated by the expression [49] given below:

$$\eta' = \frac{\int_{core} S_z dA}{\int_{all} S_z dA'} \qquad (3)$$

The amount of power fraction is symbolized by η'. The numerator part of the above equation denotes the region of interest and the denominator of the same equation performs as the whole area of the fiber.
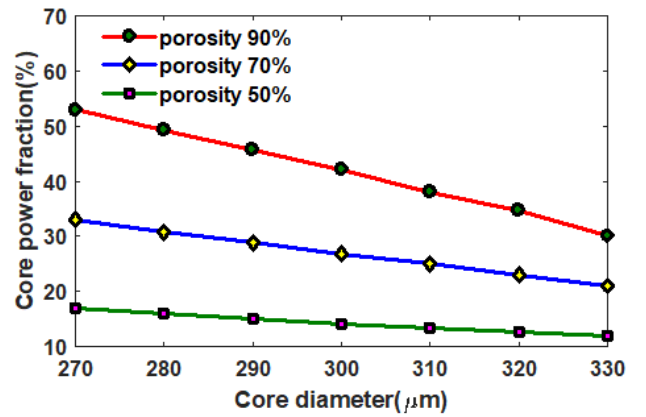

Fig. 6. Core power fraction vs core diameter at different core porosities (color online)

Fig. 5 displays at 90% and 70% porosity where core power fraction increases with frequency. But for 50% porosity increment in core power fraction is comparatively low. At higher frequency, light is tightly confined in the core which results in increased ratio of confined area to the total area of the fiber. This phenomenon has been observed in Fig. 5. By expanding the core diameter in Fig. 6, the absolute volume of air contrasted with the solid material in the core is reduced, which decreases the power fraction. At fixed diameter and frequency, the power fraction increases with core porosity which increases the amount of air inside the core. Thus, a higher amount of mode power flows through the core air slots. The core power fraction of our proposed photonic crystal fiber is 50% and 48.44%, considering x-polarization and y-polarization respectively, for 280μm core diameter and 90% core porosity.

Confinement loss is imminent in porous core PCF because air slots are used in the cladding. It is practically impossible to bind the majority of light in the core. In other words, it signifies the competence of the porous core

fiber to transmit with minimum loss. Confinement loss can be premeditated by the following equation [50]:

$$L_c = \left(\frac{4\pi f}{c} \right) \mathrm{Im}(n_{eff}) \qquad (4)$$

where, $\mathrm{Im}(n_{eff})$ indicates the imaginary part of the effective refractive index, c is the velocity of light and f is the operating frequency.
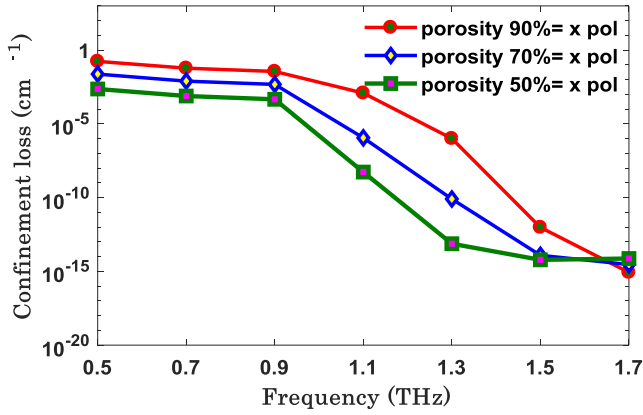

Fig. 7. Confinement loss vs. frequency at different core porosities (color online)

A standard PC-PCF must have a narrow array of confinement loss. From Fig. 7 it can be stated that confinement loss decreases as the operating frequency increases. It can be justified by the fact that at higher frequency, light bounds strongly in the core region and less light is captured by the cladding air holes. Hence the confinement loss decreases at higher operating frequency. The optimum value of confinement loss we obtained from our proposed photonic crystal fiber is 10^{-14} cm^{-1} at 50% porosities of 280 µm core diameter and 1.5 THz frequency.

V parameter is an important property for THz photonic crystal fiver. V parameter can be expressed by the following equation [51].

$$V = \frac{2\pi r f}{c} \sqrt{(n_{co}^2 - n_{cl}^2)} \le 2.405 \qquad (5)$$

η_{co} represents the refractive index of the core region and η_{cl} represents the refractive index of the cladding region, f is denoted by operating frequency and c is the speed of light in free space. Fig. 8 demonstrates the change of V-parameter as a function of frequency for different core porosities. V-parameter value of a fiber determines whether the fiber is single-mode or multi-mode. A fiber can be single-mode when its V-parameter value less or equal to 2.405.

It can be seen from Fig. 8 that our proposed fiber operates as single-mode because the value of v parameter is less than reference value. It can be confirmed that the

single mode operation of our proposed THz fiber is at 90% porosity when core diameter 280 µm and frequency less than 1.5 THz.
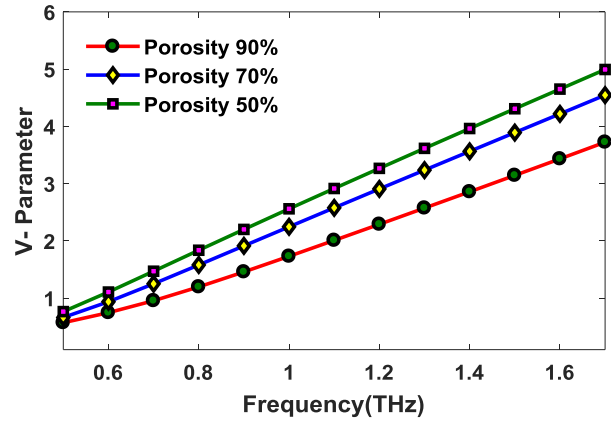

Fig. 8. V-parameter vs. frequency at different core porosities (color online)

For transmitting terahertz waveguide efficiently, low dispersion over a wide range of frequencies is a significant factor. The term dispersion is used to denote the spreading of pulses during transmission. The dispersions properties of the fiber can be calculated by the following formula [52].

$$\beta_2 = \frac{2}{c} \frac{dn_{eff}}{d\omega} + \frac{\omega}{c} \frac{d^2 n_{eff}}{d\omega^2}, \mathrm{ps/THz/cm} \qquad (6)$$

where, β_2 is the dispersion parameter, $\omega = 2\pi f$ indicates the angular frequency, c represents the speed of light in vacuum and n_{eff} indicates the effective refractive index of the proposed PCF structure.
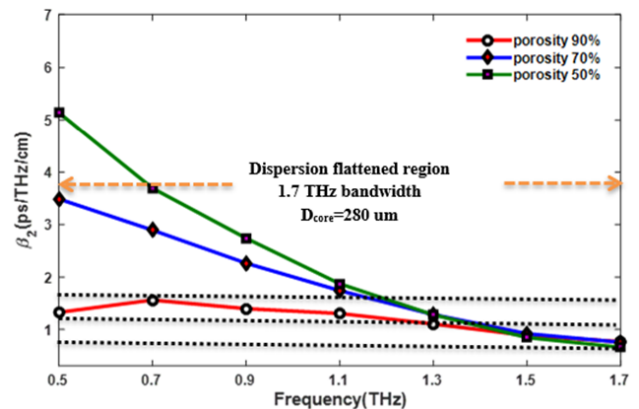

Fig. 9. Dispersion vs frequency at different core porosities (color online)

Fig. 9 displays the dispersion properties as a function of frequency. The flattened dispersion we obtained from our proposed PCF is 1.03±0.04 ps/THz/cm at a large frequency range from 0.9 THz to 1.5 THz at 90% porosity.

At higher porosity, air holes are more tightly confined resulting in less variation in refractive index.

Effective area depends on the amount of light that can be confined in the core. Effective area has been characterized by following equation [53] [54]:

$$A_{eff} = \frac{\left[\int I(r)rdr\right]^2}{\left[\int I^2(r)dr\right]^2} \qquad (7)$$

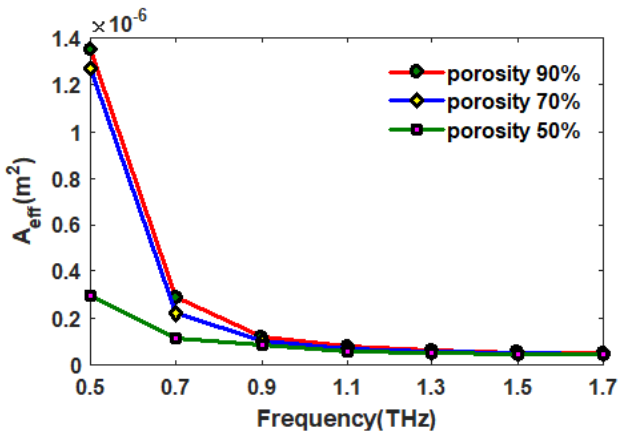where $I(r)$ is the transverse electric intensity distribution and it is characterized by $I(r) = |E_t|^2$.

Fig. 10. Effective area vs frequency
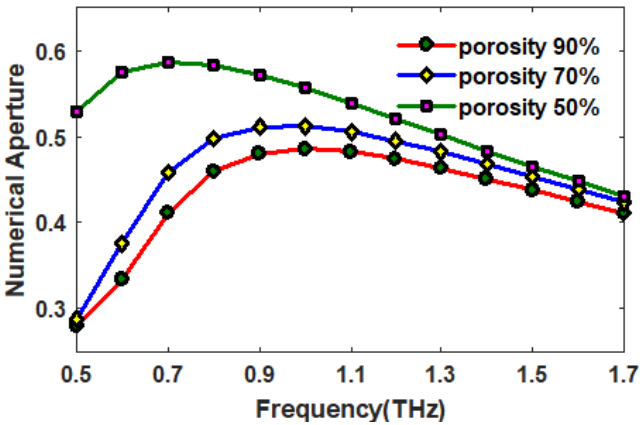*at different core porosities (color online)*

Fig. 11. Numerical Aperture vs frequency
at different core porosities (color online)

Fig. 10 shows the alteration of effective area as a function of frequency. Effective area has decreased with the increase of frequency as well as decrease of core porosity. Because at higher porosity index contrast between cladding and core increases. Eventually mode starts to expand from the core and the effective area increases. The effective area of the proposed fiber is about 1.4×10^{-6} m^2 and 1.3×10^{-6} m^2 for x-polarization and y-polarization respectively, at 90% porosity and operating frequency is at 0.5THz.

Numerical Aperture is a measure of the ability of an optical fiber to confine the incident light ray inside the core. It is another important parameter for photonic crystal fiber. This is demonstrated by following formula [55]:

$$NA = \frac{1}{\sqrt{1 + \dfrac{\pi A_{eff} f^2}{c^2}}} \qquad (8)$$

Here, A_{eff} is the effective area of the core and f is the normalized frequency and c is the speed of light. Fig. 11 demonstrates the change of numerical aperture as a function of frequency and also with porosity. At higher porosity, numerical aperture decreases with frequency.
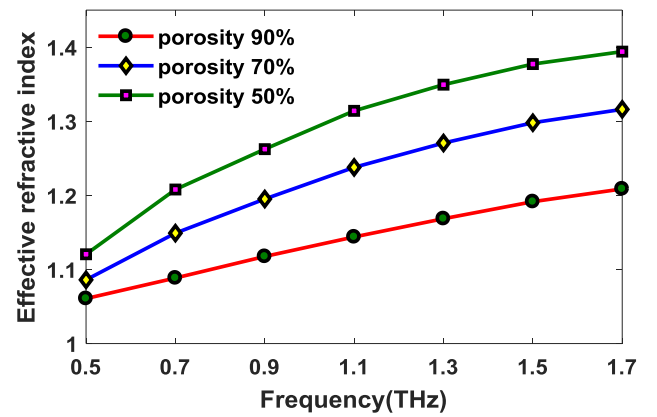

Fig. 12. Effective refractive index vs frequency
at different core porosities (color online)

The variation of effective refractive index as a function of frequency for different core porosities is shown in Fig. 12. It can be seen that the refractive index has increased with increase of frequency because at higher frequency light is confined tightly and causes the refractive index to increase. Temperature dependence is observed in the PCF, where notable effects of the acrylate coating on the birefringence are shown in [56]. Since birefringence in our proposed structure is negligible, the effect of the coating is also considered negligible.

Finally, we are comparing our proposed fiber with some recently published papers in Table 1.

4. Fabrication possibilities

Different fabrication methods have been proposed such as stacking of capillary tubes [35], casting into a mold [36], drilling the hole pattern [37] and the extrusion technique [38]. Among all these methods, the extrusion technique is considered to be most competent where preforms with macroscopic-scale (mm-scale) features are manufactured [39]. Using extrusion technique fibers with symmetric and asymmetric porous core, circular and non-circular preforms with air holes can be fabricated efficiently. Hence, we can say the proposed fiber is feasible to fabricate using existing fabrication techniques.

Table 1. Comparison of characteristics of the proposed PCF with other PCFs

Ref.	EML (cm^{-1})	Confinement Loss (L_c) (cm^{-1})	Core PF (η') (%)	Dispersion B_2 (ps/THz/cm)
[41]	0.0689	–	–	–
[42]	–	7.24 x 10^{-7}	44	0.49±0.05
[44]	0.085	4.4 x 10^{-4}	37	0.51
[45]	0.081	0.0036	46.9	0.53±0.12
[30]	0.06	9.2×10^{-3}	47	0.85±0.12
[31]	0.039	-	85	0.47±0.05
[32]	0.0492	-	43	1.7±0.05
[46]	0.07	2.30 x 10^{-3}	> 40	1.2 ± 0.32
[53]	0.066	1.24 x 10^{-13}	-	0.5 ± 0.6
[54]	0.038	-	56	0.72
[55]	0.025	1.05 x 10^{-13}	52	0.65 ± 0.05
[33]	0.007	10^{-15}	70	0.3 ± 0.1
Proposed PCF	0.029	10^{-14}	50	1.03±0.04

5. Conclusion

In conclusion, a Topaz based hexagonal circular core photonic crystal fiber is demonstrated and its guiding properties are characterized for different values of core porosities and operating frequencies in the terahertz regime. The proposed structure offers relatively low effective material loss at high porosity, very small confinement loss and a flattened dispersion profile achieved for the optimal design parameters which are suitable for efficient THz wave guidance. The structure can be manufactured due to its realistic dimension that facilitates practical fabrication. We obtained EML of 0.029 cm^{-1}, 50% core power fraction, confinement loss of 10^{-14} cm^{-1} at 90% porosity. In addition to this, we obtained near-flat dispersion of 1.03±0.04 ps/THz/cm for a wide range starting from 0.9 THz to 1.5 THz. Therefore, it is quite evident that, the proposed fiber can be a potential candidate for a long-distance terahertz wave transmission and other practical applications such as fiber-optic communication, fiber laser, non-linear devices etc. for its simple structure and significantly enhanced properties.

References

[1] J. C. Knight, T. A. Birks, P. S. J. Russell, D. M. Atkin, Optics Letters **21**(19), 1547 (1996).

[2] A. Huttunen, P. Törmä, Optics Express **13**(11), 4286 (2005).

[3] Z. Tan, X. Hao, Y. Shao, Y. Chen, X. Li, P. Fan, Optics Express **22**(12), 15049 (2014).

[4] T. V. Ramanaa, A. Pandianb, C. Ellammalc, T. Jarind, Ahmed Nabih Zaki Rashede, A. Sampath Kumar, Numerical analysis of circularly polarized modes in coreless photonic crystal fiber, Elsevier B.V. (February, 2019).

[5] J. A. West, Photonic crystal fibers, 14th Annual Meeting of the IEEE Lasers and Electro-Optics Society LEOS, 2001, (Cat. No.01CH37242).

[6] Y. Zhu, Z. He, H. Du, Sensors and Actuators B **131**(1), 265 (2008).

[7] Shiju C. Chacko, Jeena Maria Cherian, K. Sunilkumar, International Journal of Computer Applications **85**(15), (2014).

[8] N. A. Mortensen, J. R. Folken, P. M. W. Skovgaard, J. Broeng, IEEE Photonics Technology Letters **14**(8), 1094 (2002).

[9] T. Yang, E. Wang, H. Jiang, Z. Hu, K. Xie, Optics Express **23**(7), 8329 (2015).

[10] X. Tan, Y. Geng, E. Li, W. Wang, P. Wang, J. Yao, Journal of Optics A: Pure and Applied Optics **10**(8), 085303 (2008).

[11] N. H. Vu, I.-K. Hwang, Y.-H. Lee, Optics Letters **33**(2), 119 (2008).

[12] S. Ali, T. Sarkar, A. Day, M. R. Hasan, J. R. Mou, S. Rana, N. Ahmed, Ultra-low loss THz waveguide with flat EML and near zero flat dispersion properties, 2016 9th International Conference on Electrical and Computer Engineering (ICECE), 2016.

[13] Arpit Singh Yadav, Aparna Singh, Vijay Shanker Chaudhary, Dharmendra Kumar, Ultra-Flat Dispersion with High Nonlinearity Hexagonal Photonic Crystal Fiber, 2018 5th IEEE Uttar Pradesh Section International Conference on Electrical, Electronics and Computer Engineering (UPCON), (2018).

[14] P. S. Maji, Roy Chaudhuri, Optik - International Journal for Light and Electron Optics **125**(20), 5986 (2014).

[15] J. C. Knight, Science **282**(5393), 1476 (1998).

[16] P. Lin, Y. Li, T. Cheng, T. Suzuki, Y. Ohishi, IEEE Journal of Selected Topics in Quantum Electronics **22**(2), 265 (2016).

[17] H. Han, H. Park, M. Cho, J. Kim, Appl.Phys. Lett. **80**, 2634 (2002).

[18] S. Asaduzzaman, K. Ahmed, Sensing and Bio-Sensing Research **10**, 20 (2016).

[19] Y. Lu, C.-J. Hao, B.-Q. Wu, M. Musideke, L.-C. Duan, W.-Q. Wen, J.-Q. Yao, Sensors **13**(1), 956 (2013).

[20] N. Muduli, J. S. N. Achary, H. Ku. Padhy, Journal of Modern Optics **63**(7), 685 (2015).

[21] A. Argyros, Optics **2013**(7), 1 (2013).

[22] Z. L. Liu, J. An, J. W. Xing, H. L. Du, Optik International Journal for Light and Electron Optics **127**(10), 4391 (2016).

[23] G. Woyessa, A. Fasano, A. Stefani, C. Markos, K. Nielsen, H. K. Rasmussen, O. Bang, Opt. Express **24**, 1253 (2016).

[24] A. Hassani, A. Dupuis, M. Skorobogatiy, Appl. Phys. Lett. **92**, 071101 (2008).

[25] A. Dupuis, K. Stoeffler, B. Ung, C. Dubois, M. Skorobogatiy, J. Opt. Soc. Am. B **28**, 896 (2011).

[26] M. Uthman, B. M. A. Rahman, N. Kejalakshmi, A. Agrawal, K. T. V. Grattan, IEEE Photon. J. **4**, 2315 (2012)

[27] K. Tsuruda, M. Fujita, T. Nagatsuma, Opt. Express **23**, 31977 (2015).

[28] K. M. Samaun Reza, Bikash Kumar Paul, Kawsar Ahmed, Results in Physics **11**, 549 (2018).

[29] Fahad Ahmed, Subrata Roy, Kawsar Ahmed, Bikash Kumar Paul, Ali Newaz Bahar, Nano Communication Networks **19**, 26 (2019).

[30] M. A. Habiba, M. S. Anower, Optics and Spectroscopy **126**(5), 607 (2019).

[31] Izaddeen K. Yakasai, Pg. Emeroylariffion Aba, Sharafat Ali, Feroza Begum, Optical and Quantum Electronics **51**, 122 (2019).

[32] Md. Sohidul Islam, Jamilur Rahman, Mohammad Rakibul Islam, International Journal of Microwave and Optical Technology **14**(1), 62 (2019).

[33] Md. Aminul Islam, Mohammad Rakibul Islam, Zarrin Tasnim, Rakina Islam, Raisa Labiba Khan, Ehtesam Moazzam, Iranian Journal of Science and Technology, Transactions of Electrical Engineering **44**, 1583 (2020).

[34] G. Dhanu Krishna, V. P. Mahadevan Pillai, K. G. Gopchandran, Optical Fiber Technology **51**, 17 (2019).

[35] A. Dupuis, J.-F. Allard, D. Morris, K. Stoeffler, C. Dubois, M. Skorobogatiy, Opt. Express **17**, 8012 (2009).

[36] A. Dupuis, A. Mazhorova, F. Desevedavy, M. Roze, M. Skorobogatiy, Opt. Express **18**, 13813 (2010).

[37] C. S. Ponseca, R. Pobre, E. Estacio, N. Sarukura, A. Argyros, M. C. J. Large, M. A. van Eijkelenborg, Opt. Lett. **33**, 902 (2008).

[38] S. Atakaramians, S. Afshar Vahid, M. Nagel, H. Ebendorff-Heidepriem, B. M. Fischer, D. Abbott, T. M. Monro, Opt. Express **17**, 14053 (2009).

[39] Shaghik Atakaramians, V. Shahraam Afshar, Tanya M. Monro, Derek Abbott, Advances in Optics and Photonics **5**(2), 169 (2013).

[40] Ahmed, Kawsar, Sawrab Chowdhury, Bikash Kumar Paul, Md Shadidul Islam, Shuvo Sen, Md. Ibadul Islam, Sayed Asaduzzaman, Applied optics **56**(12), 3477 (2017).

[41] Islam Md Saiful, Jakeya Sultana, Alex Dinovitser, Brian W-H. Ng, Derek Abbott, Optics Communications **413**, 242 (2018).

[42] Luo, Jianfeng, Fengjun Tian, Hongkun Qu, Li Li, Jianzhong Zhang, Xinhua Yang, Libo Yuan, Applied optics **56**(24), 6993 (2017).

[43] Wu, Zhiqing, Xiaoyan Zhou, Handing Xia, Zhaohua Shi, Jin Huang, Xiaodong Jiang, Weidong Wu, Applied optics **56**(8), 2288 (2017).

[44] M. A. Habib, M. S. Anower, Optical Fiber Technology **47**, 197 (2019).

[45] Mohammad Rakibul Islam, Md. Faiyaz Kabir, Khandoker Md. Abu Talha, Md. Saiful Islam, Sensing and Bio-Sensing Research **25**, 100295 (2019).

[46] M. S. Islam, S. Rana, M. R. Islam, M. Faisal, H. Rahman, J. Sultana, PIET Commun. **10**, 2179 (2016).

[47] Na-Na Chen, Jian Liang, Li-Yong Ren, Appl. Opt. **52**(21), 5297 (2013)

[48] Md. Moshiur Rahman, Farhana Akter Mou, Mohammed Imamul Hassan Bhuiyan, Mohammad Rakibul Islam, Optical Fiber Technology **55**, 102158 (2020).

[49] Farhana Akter Mou, Md. Moshiur Rahman, Mohammad Rakibul Islam, Mohammed Imamul Hassan Bhuiyan, Sensing and Bio-Sensing Research **29**, 100346 (2020).

[50] K. I. Zaytsev, J. Phys. Conf. Ser. **486**(1), 012014 (2014).

[51] Mohammad Rakibul Islam, Md. Faiyaz Kabir, Khandoker Md. Abu Talha, Md. Shamsul Arefin, Optical Engineering **59**(1), 016113 (2020).

[52] J. Sultana, Md S. Islam, M. R. Islam, D. Abbott, Electronics Letters **54**, 61 (2017).

[53] B. K. Paul, M. A. Haque, K. Ahmed, S. Sen, Photonics **6**, 32 (2019).

[54] B. K. Paul, K. Ahmed, Opt. Mater. **100**, 109634 (2020).

[55] Md. Aminul Islam, M. Rakibul Islam, Md. Moinul Islam Khan, J. A. Chowdhurya, F. Mehjabin, Mohibul Islam, Physics of Wave Phenomena **28**(1), 58 (2020).

[56] Y. H. Kim, K. Y. Song, Journal of Lightwave Technology **33**(23), 4922 (2015).

_____

*Corresponding author: rakibultowhid@yahoo.com